Accepted Manuscript

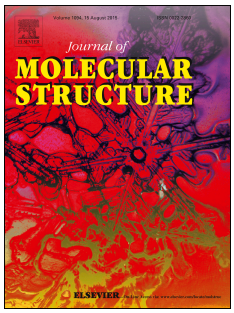

Probing mechanism of α-formylketene dithioacetal towards the facile formation of functionalised pyrimidines: A structural approach

Monu Joy, Adebayo A. Adeniyi, Annie Mathews, Bijo Mathew, S. Prasanth, Mohmoud E.S. Soliman, Jalaja J. Malayan, E.R. Anabha

PII: S0022-2860(16)30791-8

DOI: 10.1016/j.molstruc.2016.07.107

Reference: MOLSTR 22810

To appear in: *Journal of Molecular Structure*

Received Date: 6 May 2016

Revised Date: 25 July 2016

Accepted Date: 27 July 2016

Please cite this article as: M. Joy, A.A. Adeniyi, A. Mathews, B. Mathew, S. Prasanth, M.E.S. Soliman, J.J. Malayan, E.R. Anabha, Probing mechanism of α-formylketene dithioacetal towards the facile formation of functionalised pyrimidines: A structural approach, *Journal of Molecular Structure* (2016), doi: 10.1016/j.molstruc.2016.07.107.

Graphical Abstract

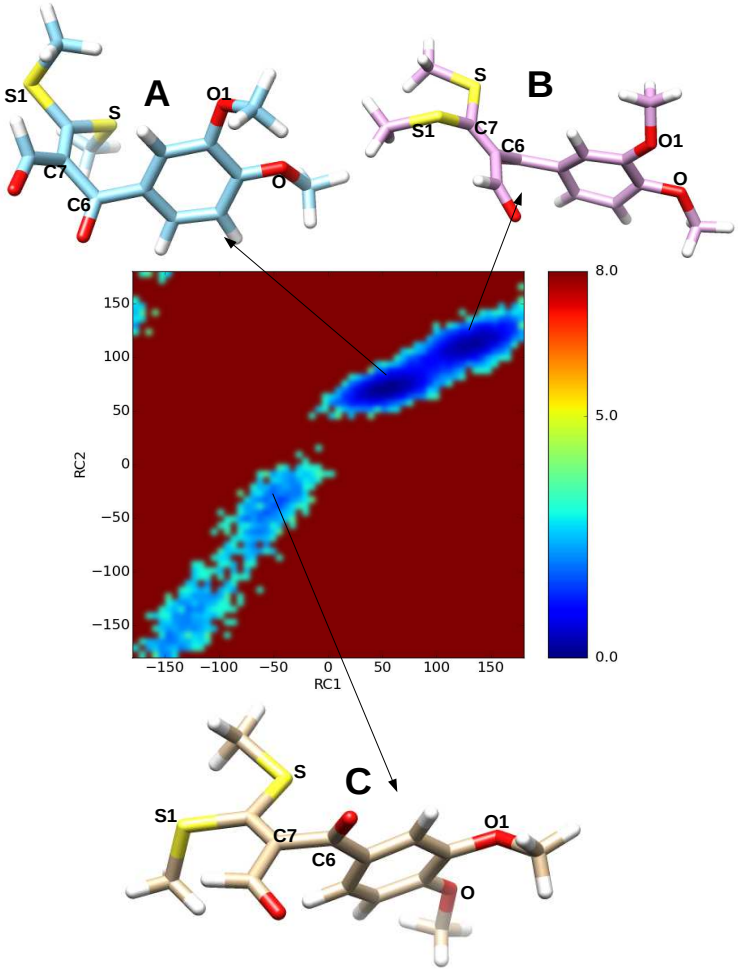

Probing mechanism of α- Formylketene dithioacetal towards the facile formation of functionalised pyrimidines: a structural approach

Monu Joy[a,d*], Adebayo A. Adeniyi[b], Annie Mathews[a], Bijo Mathew[c], S Prasanth[d], Mohmoud E.S. Soliman[b], Jalaja J Malayan[a], E R Anabha[e]

[a]Department of Chemistry, Baselius College, Kottayam-686001, Kerala, India

[b]School of Health Science, University of KwaZulu-Natal, Westville, Durban 4001, South Africa

[c]Division of Drug Design and Medicinal Chemistry Research Lab, Department of Pharmaceutical Chemistry, Ahalia School of Pharmacy, Palakkad -678557, Kerala, India

[d]School of Pure & Applied Physics, MG University-686560, Kerala, India

[e]Department of Chemistry, Sree Narayana College, Thrissur-680566, Kerala, India

Abstract

α-Formylketene dithioacetal is an active precursor for the synthesis of a variety of organic compounds including pyrimidines and its functionalized materials. The present study deals with the structural versatility of a solid representative compound from the family of α-formylketene dithioacetal to the formation of functionalized pyrimidines derivatives through experimental as well as theoretical methods. 2-(3,4-dimethoxybenzoyl)-3,3-bis(methylsulfanyl)prop-2-enal, the representative compound was synthesized with a reported protocol and characterized through spectral methods. The complete three dimensional solid state structural studies were carried out utilizing single crystal X-ray crystallographic technique along with theoretical methods like classical and accelerated molecular dynamics simulation. Various quantum chemical parameters were also discussed to reveals the complete molecular geometry and reactivity of designated compound.

Formyl ketene dithioacetal; Pyrimidine; Single Crystal XRD; Molecular Dynamics, Quantum Chemical Calculations

[*]Corresponding and first author: (Present address)

Monu Joy
School of Pure & Applied Physics
MG University-686560
Kerala, India

1. Introduction

α- Formylketene dithioacetals are multifarious starting materials for the synthesis of number of heterocyclic compounds such as pyridines and nicotinonitriles [1]. They can be prepared by the reaction of ketones containing active methelene group with carbon disulfide in the presence of a strong base like sodium *ter*-butoxide and subsequent alkylation to generate ketene dithioacetals and then the formylation of the corresponding ketene dithioacetal with 1.5 equivalents of Vilsmeier- Haack reagent [2]. The aldehydic moiety is stabilized through conjugation of π electrons towards the aromatic region where as the formylation will not performed over aliphatic ketene dithioacetals via Vilsmeir – Haack approach [2, 3].

Scheme 1

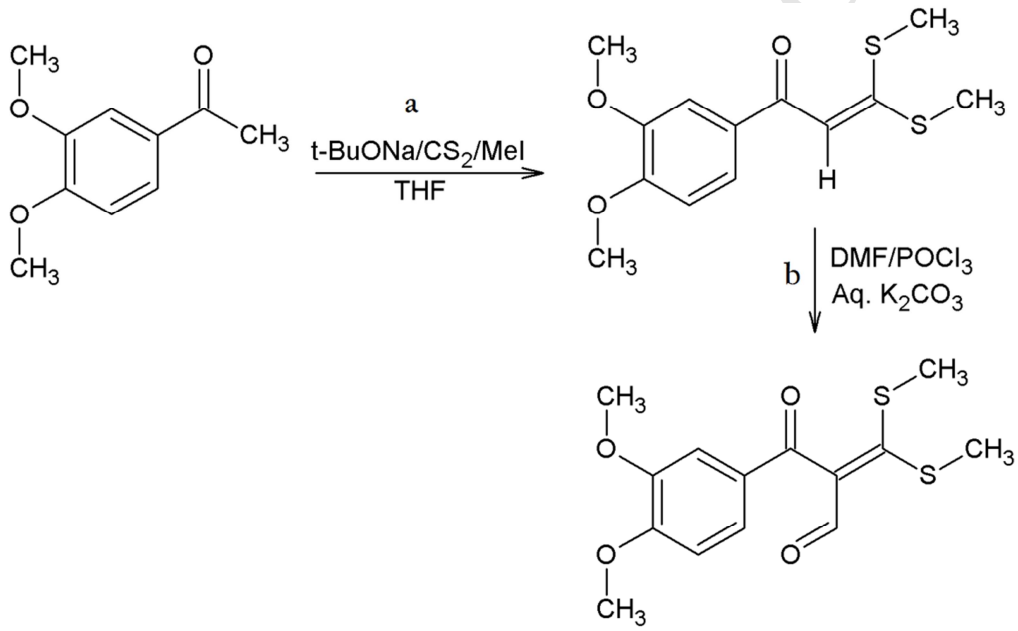

It is a doubly activated unique building block because of the presence of both ketonic and aldehyde functional groups in addition to the ketene dithioacetal moiety at the α-position. As each of these three groups has varying reactivity towards condensing agents, their selectivity can be utilized effectively for the synthesis of a wide variety of substituted and annulated heterocycles [2, 4]. One of the vital class of compounds that can be synthesized from α-formylketene dithioacetals is pyrimidine derivatives; they demonstrate a diverse array of biological and pharmacological activities including anticonvulsant, antibacterial, antifungal, antiviral and anticancer properties [5, 6]. Pyrimidine-5-carbaldehydes are valuable precursors for the synthesis of drugs used for the treatment of *Alzheimer* disease [7]. Some annulated pyrimidines are used in the treatment of cardiovascular diseases [8] and insomnia [9]. It is important to learn the electronic structure and its reactivity of the α-formylketene dithioacetal

towards the formation of pyrimidine derivatives and also it is possible to establish the optimum criteria for the synthesis of further useful pyrimidine derivatives in future. So here we reveal the structural adaptability of 2-(3,4-dimethoxybenzoyl)-3,3-bis(methylsulfanyl)prop-2-enal (Mol1) towards the one pot formation of pyrimidines through experimental and theoretical electronic structure. From the light of above view, herein we establish the complete X-ray crystallographic, classical and accelerated molecular dynamics (AMD) and quantum chemical properties of Mol1, one of the crystalline α-formylketene dithioacetals obtained through Vilsmeir–Haack reaction on 3,4-dimethoxybenzoylketene dithioacetal following the procedure of Asokan *et al* [2] as an extension of our interest in sulfur containing compounds [10]. To the best of our knowledge neither detailed theoretical calculation nor detailed crystallographic parameters of this compound have been reported yet.

2. Experimental

2.1 Synthesis

Mol1 had been synthesized with a reported method [2]. 3,4-dimethoxy acetophenone 18mg (0.1M) was dissolved in CS_2 (7mL, 0.1M) and it was added dropwise to an ice-cold suspension of sodium *t*-butoxide (0.2M) in dry THF. The reaction mixture was allowed to stir for 5-6 hours. After 6 hours 29mL of methyl iodide (0.2M) was added dropwise. The temperature should be 0 to 5°C. The reaction mixture was allowed to stand for 10 hours, reaction was quenched by adding water and the product is extracted using ethyl acetate, dried over anhydrous sodium sulphate (Scheme 1a). The α-oxoketene dithioacetal was purified by column chromatography using 2:8 ethyl acetate-hexane mixture solution. The purified ketene dithioacetal was treated with Vilsmeier-Haack reagent as follows. 14.2g of α-oxoketene dithioacetal(0.05M) was treated with 1.5 equivalent of $POCl_3$ in dry DMF at -5 to 0°C, to obtain the title compound with 80% yield (Scheme 1b). The compound was purified using column chromatography with 3:7 ethyl acetate-hexane solution and was crystallized using the same solution through slow evaporation. FT-IR spectrum was recorded using thermo Nicolet, Avatar 370 FT-IR Spectrometer equipped with a deuterated triglycine sulfate detector with spectral range 4000-400 cm^{-1} and resolution 4 cm^{-1}. FT-Raman spectrum was recorded from Bruker RFS 27: Stand alone FT-Raman Spectrometer with a scanning range of 50-4000 cm^{-1} and a resolution of 2 cm^{-1} with a laser source of Nd: YAG 1064 nm. FT-NMR (^1H and ^{13}C) spectrum was taken in $CDCl_3$ solution at room temperature and all signals were referenced to TMS on a Bruker AVANCE III-(400MHz for ^1H and 100MHz for ^{13}C) FT-NMR Spectrometer. 2-(3,4-dimethoxybenzoyl)-3,3-bis(methylsulfanyl)prop-2-enal, pale yellow

coloured crystals; mp 108-110°C; yield: (86%); IR (FT) ν_{max} / cm^{-1} 600, 1275, 1578, 1634, 1662, 2822, 2938, 2999; RAMAN (FT) ν_{max} / cm^{-1} 1507, 1588, 1656, 2931; ^{1}H NMR (400MHz, $CDCl_3$): δ = 2.56, 2.46 (2s, 6H, methyl sulfanyl); 3.94 (s, 6H, dimethoxy); 6.85-7.55 (m, 3H aromatic); 10.17 (s, 1H, aldehydic) ppm. ^{13}C NMR (100MHz, $CDCl_3$): δ = 17, 18 (methyl sulfanyl); 56 (methoxy); 129 (aliphatic sp^2 hybridised); 121, 124, 132, 141,149, 154 (aromatic); 186 (ketonic); 192 (aldehydic) ppm.

2.2 Data Collection & Refinement

Single crystals of the compound suitable for X-ray diffraction were grown by slow evaporation from ethyl acetate-hexane solution. The yellow crystals were prismatic. The dimensions of the crystal used for data collection were 0.20 x 0.30 x 0.35 mm^3. The crystals belonged to Monoclinic system having space group P21/n with unit cell dimensions, a = 8.6760Å, b = 16.0399Å, c = 11.2260Å, α = 90°, β = 102° and γ = 90°. Data were collected using Brucker AXS Kappa Apex II CCD detector diffractometer using graphite monochromatic Mo-Kα radiation (λ=0.71073Å) at 293K. The data reduced using the program SAINT [11] and empirical absorption corrections are done using the SADABS [12]. The structure was solved by intrinsic phasing method using SHELXT-2013 [13]. The top 21 peaks formed the complete structure. The structure was refined using full-matrix least squares method based on F^2 using SHELXL-2013 [14]. Five cycles of isotropic refinement were followed by anisotropic refinement for the non-hydrogen atoms. The position of all hydrogen atoms were geometrically fixed and treated with riding atoms, with C-H distances of 0.93 or 0.96 Å. Anisotropic refinements of the non-hydrogen atoms along with isotropic refinement of hydrogen atoms has been carried out using 4990 reflections. Materials for publications were prepared using, ORTEP [15], Mercury [16] programs. Detailed crystallographic data for the structural analyses have been deposited with the Cambridge Crystallographic Data Centre, CCDC with deposition number 1422213. Copies of this information can be obtained from The Cambridge Crystallographic Data Centre, 12 Union Road, Cambridge CB21EZ, UK (fax: +44-1223-336033; e-mail: deposit@ccdc.cam.ac.uk or www: http://www.ccdc.cam.ac.uk).

2.3 Classical and Accelerated Molecular Dynamics

The crystallographic geometry was exploited to optimize the molecule using Gaussian 09[17] with functional/basis set of HF/6-31G* and the force field as well as atomic charges were computed and fitted through the supporting package RED[18]. Parameterization was done using the restrained electrostatic potential (RESP) method as implemented in the package RED to fit the atomic partial charges of the atoms. The solute was immersed in an

orthorhombic solvent box mixture of 20% acetonitrile and 80% water as an explicit solvent system [19] using the package pyMDMix version 0.2 (http://mdmix.sourceforge.net). Molecular dynamics was done using Amber 12 [20] and GPU based PMEMD programme [21]. Partial mesh ewald (PME) method was used for the long range electrostatic potentials with vdW cut-off of 12Å. Two level of minimization was done, first with strong constrained on the molecule for 1000 steps (500 steepest descent followed by 500 steps of conjugate gradient) and the second without constraint for 1000 steps of conjugate gradient only. The system was gradually heated up to temperature of 300K in canonical ensemble for 50ps using Langevin thermostat with a collision frequency of $1ps^{-1}$ and a harmonic restrained of 5 kcal/mol Å on the solutes. The density of the system was equilibrated for another 50ps in NPT ensemble and the final equilibration at 300K temperature, 1bar pressure and a coupling constant of 500ps was carried out for 500ns which were finally followed by 10ns production MD. In all the steps of simulations, frame were recorded at every 500 steps of simulation and a time step of 2fs and all bond lengths involving hydrogen atoms were restrained with SHAKE algorithm [22]. In order to sufficiently sample the possible conformational minimal of the molecule, we applied the accelerated molecular dynamic simulation (AMD) methods [23] for another 10 ns.

2.4 Quantum chemical details

The molecular geometry optimization, calculations of energy and various quantum chemical reactivity descriptors were carried out for Mol1 in an acetonitrile solvent system with the Gaussian 09W [17] software package using DFT/B3LYP functional combined with the standard 6-311G(d,p) basis set. DFT employed the B3LYP keyword which invokes Becke's three parameter hybrid method [24, 25] using correlation function of Lee *et al*. HOMO–LUMO analysis was carried out in gas phase with B3LYP/6-311G(d,p) to explain the charge transfer within the molecule. Ionization Potential (IE), Electron Affinity (EA), Global Electronegativity (χ), Chemical Hardness (η), Chemical Softness (S), Chemical Potential (μ), Global electrophilicity index, Dipole Moment (Debye) have been calculated using the highest occupied molecular orbital (HOMO) and lowest unoccupied molecular orbital (LUMO). The NBO analysis was performed using the Gaussian 09W package at the B3LYP/6-311++G(d,p) level in order to understand various second order interactions between the filled orbital's of one subsystem and vacant orbital's of another subsystem, which is a measure of the intra-molecular delocalization or hyper conjugation [26]. Mulliken population analyses have been calculated. Molecular electrostatic potential (MEP) analysis has been used to find the reactive sites of the compound. The electrostatic potential contour

map with the negative regions (assigned to red) of MEP were related to electrophilic attacks and positive regions (assigned to blue) were related to nucleophilic reactivity. Fukui functions and molecular electrostatic potential (MEP) were evaluated and analysed with mPWIPW91/6-311G(d,p) level of theory.

3. Result & discussion

3.1 Spectral description

The IR data shows a peak at 2999cm^{-1} representing aromatic C-H stretching vibration. Carbonyl stretching vibrations are visible at 1662 & 1634cm^{-1}. Peak at 1578cm^{-1} corresponds to aromatic C=C double bond stretching vibration. Peak at 1275cm^{1} reveals C-O vibration in the methoxy group. C–S vibration is visible at 600cm^{-1}. C-H vibrations corresponds to methoxy group is at 2822cm^{-1} where as simple methyl group vibrates at 2938cm^{-1}. The RAMAN spectrum represents a peak at 2931cm^{-1} represents the aromatic C-H stretching vibration. The peak at 1656cm^{-1} corresponds to carbonyl frequency. 1588cm^{-1} belongs to the aromatic C=C vibration. Aromatic C-C vibration is lying at 1507cm^{-1}. An intense peak obtained between 100 and 125cm^{-1} shows the lattice vibration reveals the crystalline nature of the compound. The ^{1}H NMR data show peaks at 2.56 and 2.46 ppm which can be assigned to six protons of methylsulfanyl group. The peaks lying between 6.85-7.55 ppm represent three aromatic protons and the peak at 3.94 ppm represents the 6 protons of two methoxy groups attached on the benzene ring. The aldehydic proton is at 10.17ppm. The ^{13}C NMR having a peak at 192ppm represents aldehydic carbon and 186ppm for ketonic carbon. Peak at 17 and 18ppm corresponds to two methyl sulfanyl carbons whereas methoxy carbons lying at 56 ppm. The characteristic peaks between 121-154 ppm represent 6 aromatic carbons. The peak corresponds to aliphatic double bonded carbon is observed at 129 ppm.

3.2 Crystallographic studies

The crystal data and structure solution details of the compound are given in **Table 1**.

Table 1

Empirical formula	C_{14} H_{16} O_4 S_2	
Formula weight	312.41	
Temperature	293(2) K	
Wavelength	0.71073 Å	
Crystal system	Monoclinic	
Space group	P 21/n	
Unit cell dimensions	a = 8.6760(3) Å	a= 90°.
	b = 16.0399(4) Å	b= 102.093°
	c = 11.2260(4) Å	g = 90°.

Volume	1527.57Å^3
Z	4
Density (calculated)	1.358 Mg/m^3
Absorption coefficient	0.336 mm^{-1}
F(000)	544
Crystal size	20 x 30 x 35 mm^3
Reflections collected	11708
Independent reflections	3766 [R(int) = 0.0223]
Completeness to theta	25.242°, 99.9 %
Refinement method	Full-matrix least-squares on F^2
Data / restraints / parameters	3766 / 0 / 181
Goodness-of-fit on F^2	0.966
R1 = 0.0370, wR2 = 0.1056	

Crystal data

Figure 1

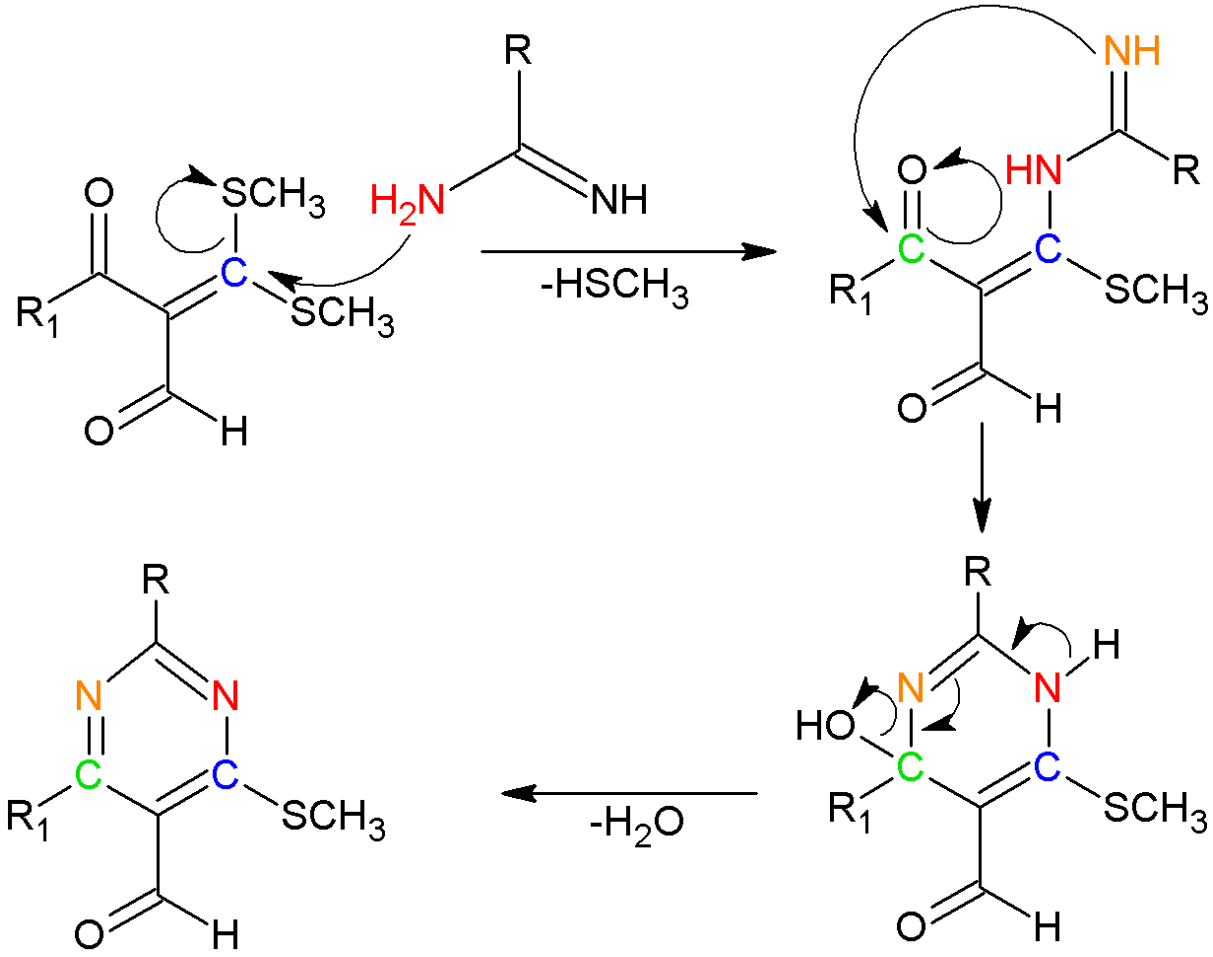

Mechanism of formation of pyrimidines from α- Formylketene dithioacetals

The ORTEP diagram of the Mol1 is shown in **Fig: 2** and the details of the data collection specification and the parameters of the refinement are given in **Table 1.** Because of the substitutions, the phenyl ring appears little distorted and angles are slightly out of hexagonal structure ∠C3-C1-C2 119.5°, ∠C2-C4-C6 120.0°, ∠C4-C6-C5 119.8°, ∠C1-C3-C5 120.7°, ∠C1-C2-C4 119.9° and the bond lengths ranges from 1.379 Å to 1.410 Å .

Figure 2

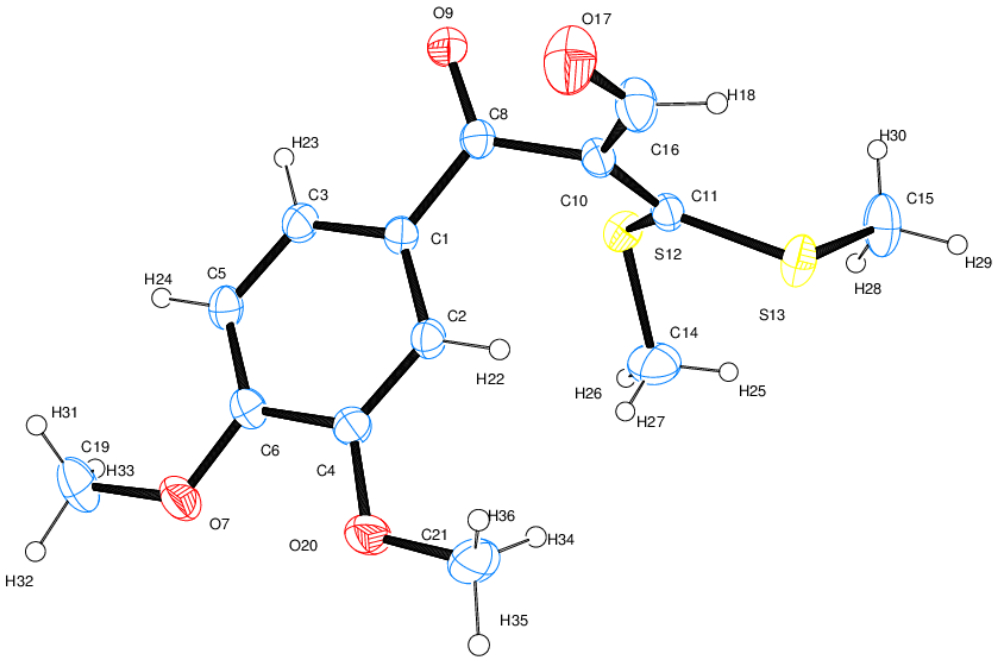

ORTEP diagram of the Mol1 with 50% polarisability

Two methoxy groups attached to the phenylic moiety and the phenyl group itself are coplanar in nature as observed from the structure. Ketonic carbonyl group is slightly out of plane as compared to the phenylic residues ∠O9-C8-C1-C3 12.7°. The methoxy substitution contributes the crystalline nature via its triangular binding by means of its electron releasing capacity through conjugation. It is proved because similar aroyl substituted formyl ketene derivatives are semi solids [2]. Short inter molecular attraction of methoxy group and methyl sulfanyl hydrogen help the three dimensional architecture of the crystal through non covalent interaction as shown in the **Fig: 3**. An intra molecular hydrogen bonding pattern is depicted by C-H…O and C-H…S interactions (**Table 2**) are also responsible to the three dimensional architecture of the molecule in the monoclinic system.

Table 2. Hydrogen bonding interactions of for Mol1.

D-H...A	d(D-H) Å	d(H...A) Å	d(D...A) Å	<(DHA) °
C(19)-H(33)...S(12)$^{\#1}$	0.96	3.02	3.938(2)	161.4
C(15)-H(29)...O(17)$^{\#2}$	0.96	2.63	3.515(2)	153.8
C(14)-H(27)...O(20)$^{\#3}$	0.96	2.58	3.347(2)	137.0
C(14)-H(27)...O(7)$^{\#3}$	0.96	2.59	3.339(3)	134.6
C(5)-H(24)...O(9)$^{\#1}$	0.93	2.45	3.3678(18)	168.9

d: distance; D: Donor; A: Acceptor; H: Hydrogen

Symmetry transformations used to generate equivalent atoms:
$^{\#1}$ x+1/2,-y+1/2,z+1/2; $^{\#2}$ x-1,y,z; $^{\#3}$ -x,-y,-z+2

Figure 3

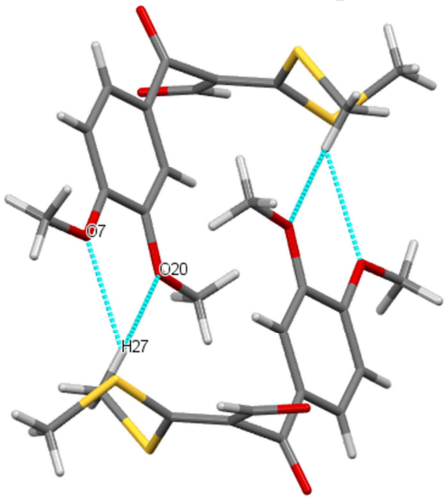

Triangular interaction of methoxy oxygen with methyl sulfanyl hydrogen

The feasibility of formation of pyrimidines from formyl ketenedithioacetal using amidines can be rationalized according to the mechanism proposed by Topfl *et al* [27]. The quantitative study of the same could be reveals here through its crystal structure: The methyl sulphanyl groups are oriented in such a way as to avoid the steric interaction between them in accordance with the torsion angles ∠C14-S12-C11-S13 44.6°, ∠C15-S13-C11-S12 42.8° leading to the ease of formation of an acyclic N,S-acetal on addition with an amidine, and one of the two methyl sulfanyl groups are susceptible for leaving as methyl thiol because C10-C11 bond is rotatable. The dimethoxy acetophenone moiety with its extensive conjugation helps the polarization of ketonic carbonyl group rather than aldehydic carbonyl, favors the

formation of cyclic intermediate via intramolecular 1,2-nucleophilic amination reaction. Electron releasing effect of two methoxy groups on acetophenon facilitates the conjugation of the precursor as evident by the partial double bond character C10…C11 1.35 Å, C2…C4 1.37 Å and C3…C5 1.38 Å and partial single bond character C10…C16 1.46 Å, C8…C10 1.50Å, C1…C8 1.48 Å, C1…C2 1.40 Å and C4…C6 1.41 Å but the conjugation is not extended to the methyl sulfanyl groups S12…C14 and S13…C15 are 1.79 Å. The aldehydic group appears completely out of plane from the rest of the residues, is due to the interaction (**Fig. 4**) of aldehydic oxygen with methyl sulfanyl hydrogen and aldehydic hydrogen may leads to unreacted on the formation of pyrimidines make it as a synthon for highly useful functional pyrimidine derivatives.

Figure 4

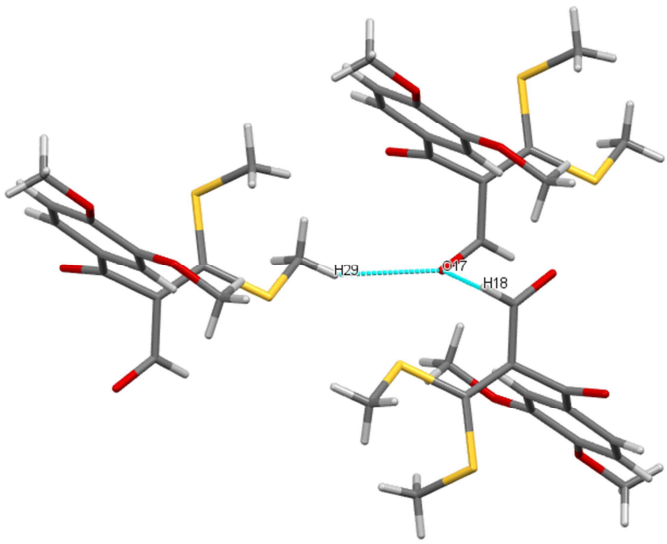

Interaction of aldehyde oxygen with methyl sulfanyl hydrogen and aldehydic hydrogen

3.3 Molecular Dynamics simulation

X-ray crystallographic structure represents one frozen view of the molecule; whereas all possible conformations are available in solution along with solvent effects. Acetophenone or DMF is the solvent used in the formation of pyrimidines from α-Formylketene dithioacetals but former gives higher yield [28]. Inclusion of solvent effects along with a dynamic nature of the molecule is only given by Molecular Dynamics simulation and the AMD is the best method for conformational minimal search. Herein we performed both classical and AMD simulations for searching any possible conformations that are available over a time period of 10ns. Throughout the 10ns classical molecular dynamics simulation,

there is no observed change in the root means square displacement (RMSD) of the Mol1 but significant changes was observed during the AMD simulation. The kinetic (EKTOT), potential (EPTOT) and total (ETOT) energies for the 10 ns classical MD of the compound are shown in **Fig: 5a** while the corresponding ones obtained through the AMD simulation are shown in **Fig: 5b**. These plots clearly show that both classical and accelerated molecular dynamics have similar EKTOT, EPTOT and ETOT surface and stable energy equilibrium was observed in the two methods.

Figure 5a

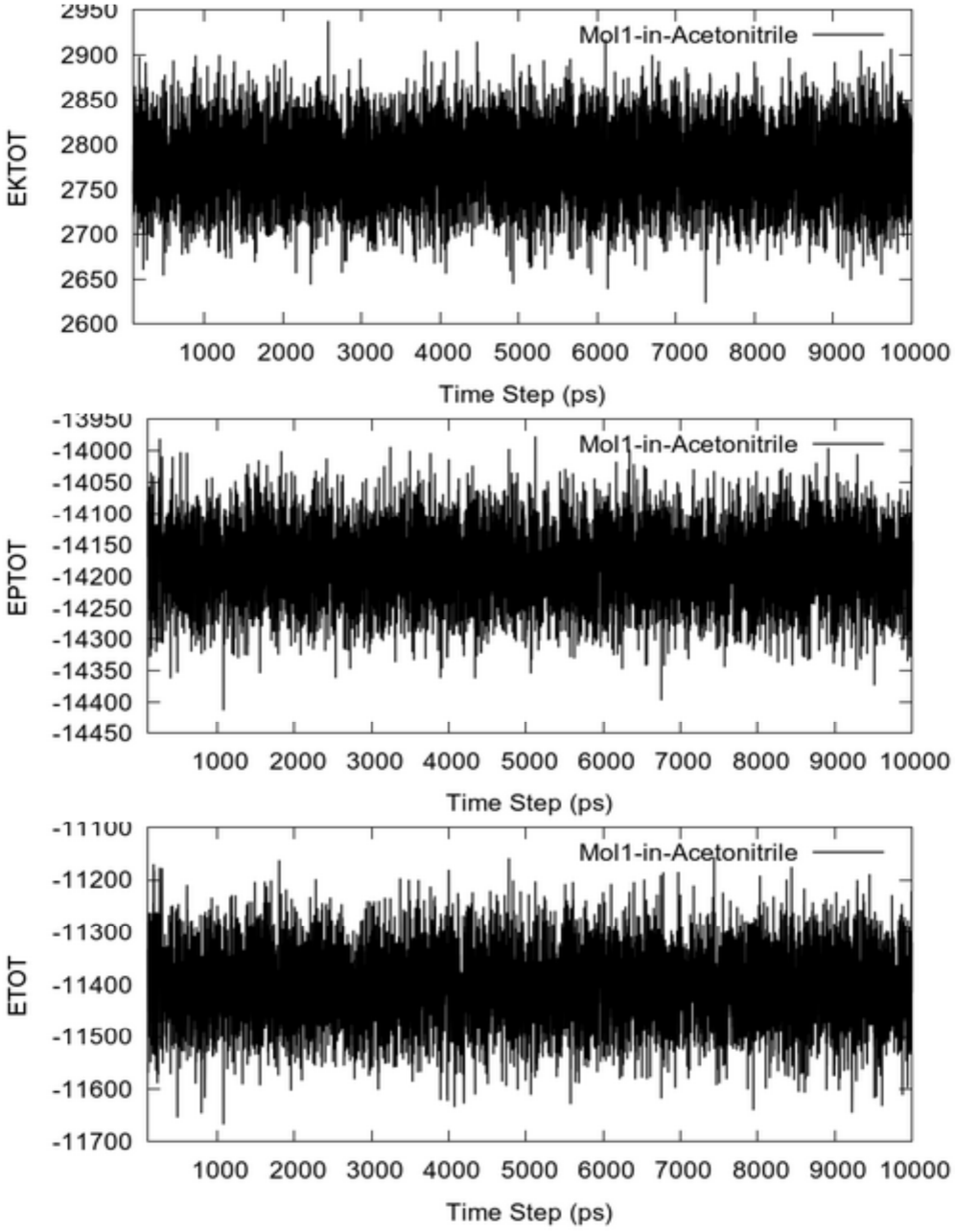

The kinetic, potential and total energies of the ligand for the 10 ns of molecular dynamics

Figure 5b

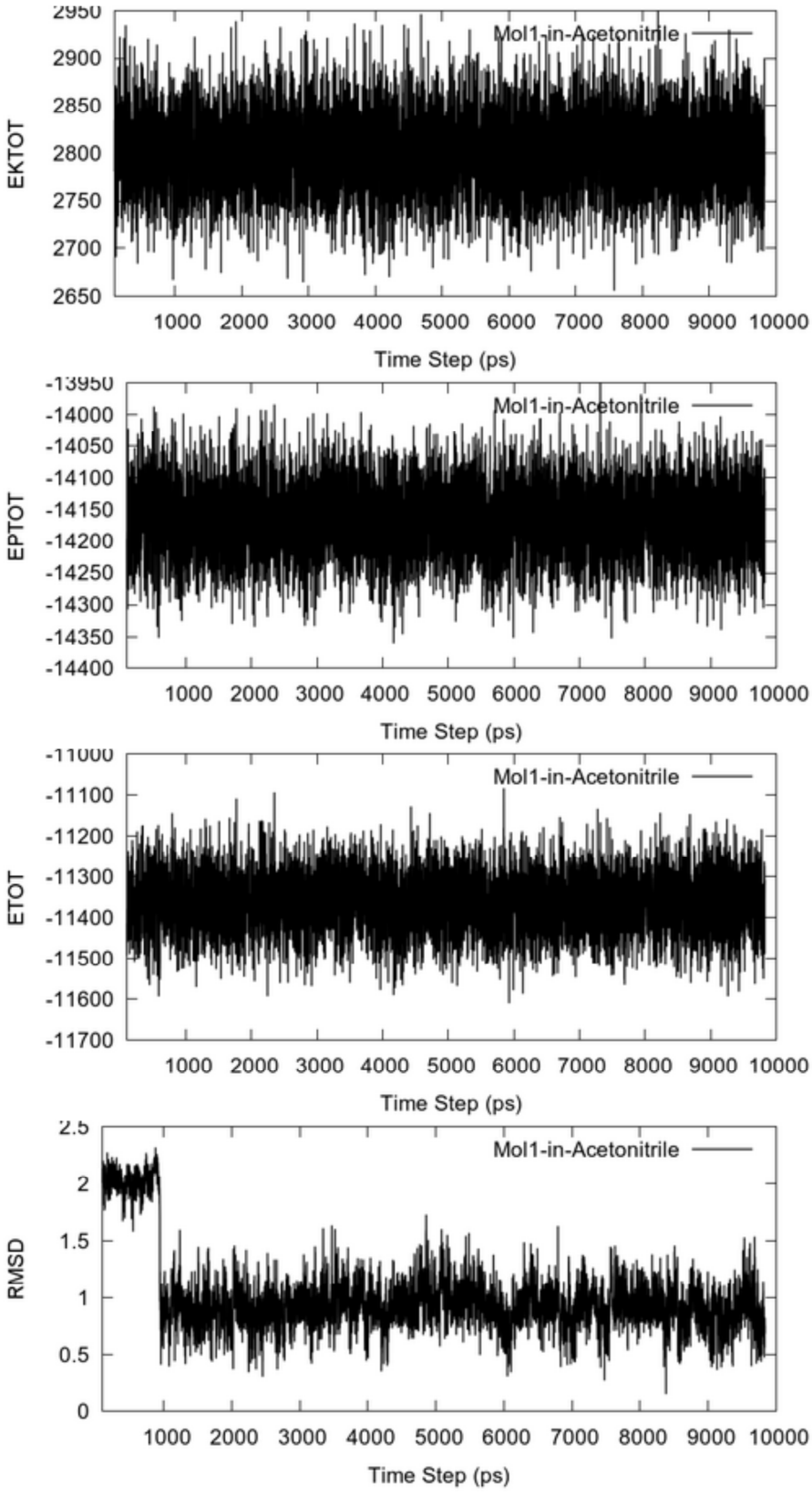
EKTOT
Mol1-in-Acetonitrile
Time Step (ps)
EPTOT
Mol1-in-Acetonitrile
Time Step (ps)
ETOT
Mol1-in-Acetonitrile
Time Step (ps)
RMSD
Mol1-in-Acetonitrile
Time Step (ps)

The kinetic, potential, total energies and RMSD of the ligand for the 10 ns of accelerated molecular dynamics

After the 10 ns of classical MD simulation, the structure of the compound interacting with the solvent molecules of acetonitrile (ANT) and water (WAT) within the range of radius less than 4 Å is shown in **Fig: 6**. Both acetonitrile and water molecule do not have any HB interaction with the ligand but they both exhibit a vDw contact within the range of -0.2 to -0.4 as shown in **Table 3**.

Figure 6

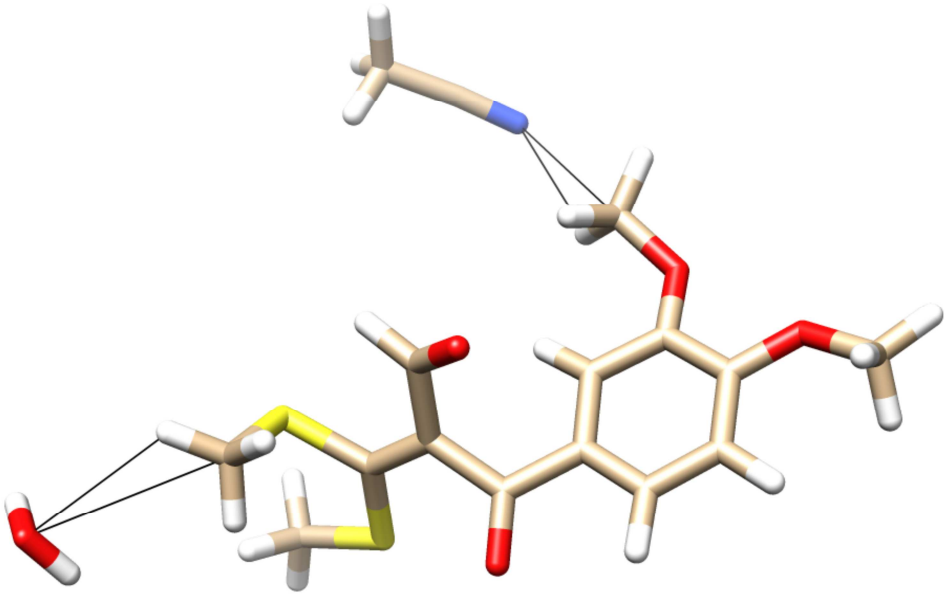

The vDw interaction of solvent molecules (water and acetonitrile) with the ligand after the 10 ns simulation steps.

Table 3

Ligand atom	Solvent atom	vDw	Distance
LIG 1 C13	ANT 211 N1	-0.238	3.563
LIG 1 H14	ANT 211 N1	-0.272	2.897
LIG 1 H8	WAT 236 O	-0.376	2.876
LIG 1 C10	WAT 236 O	-0.381	3.581

The Vdw contact interaction of the solvent molecules (ANT and WAT) with the Mol1

The geometry of the ligand remains virtually the same after the 10ns of classical MD simulation without any root means square displacement (RMSD) reveals the stability of the conformation within the solvent system. In order to explore the conformational space for any possible geometrical minimal, the AMD method was applied as described in the methodology. After the 10 ns of AMD simulation, three additional conformations of the compound were identified as local minimum as shown in **Fig: 7**. The conformational changes in the ligand were determined in terms of the changes in the selected two dihedral angles O-C6-C7-S1 (RC1) and O1-C6-C7-S (RC2) as shown in **Fig: 7**. The energy surface clearly shown that three more minimal geometries of the ligand were obtained in the order of A > B > C respectively in terms of the potential energy surface as shown in Table 4.

Figure 7

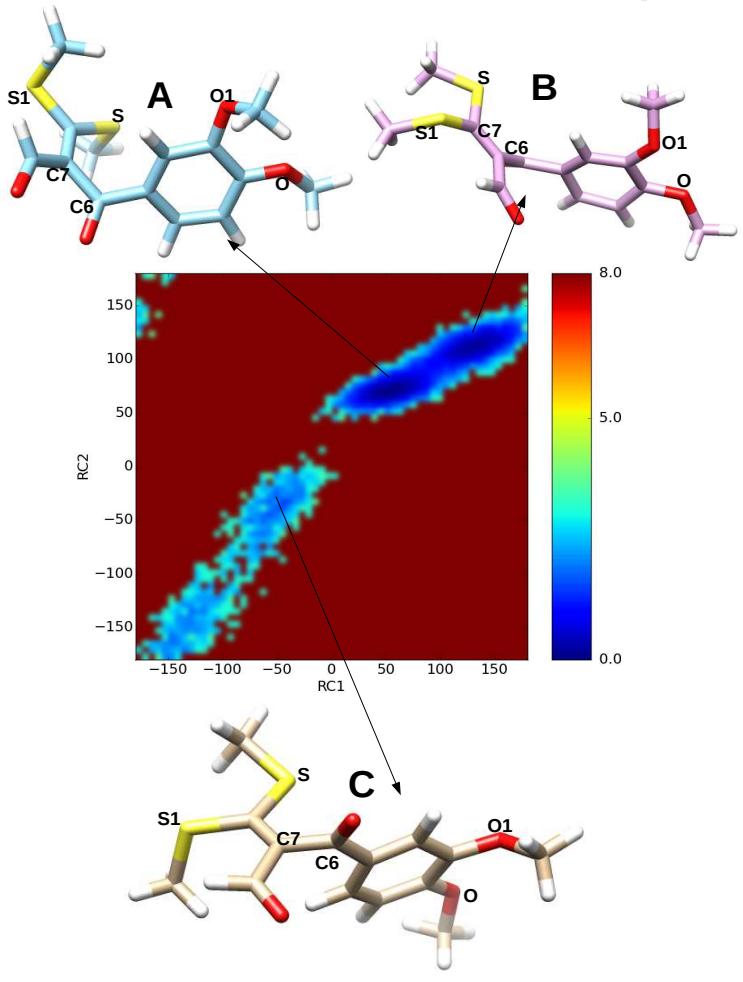

The conformational minimal's of the ligand obtained through the AMD simulation

Table 4.

Step (ps)	State	RC1 (Degree)	RC2 (Degree)	PMF(kcal/mol)	RMSD from initial geometry (Å)
0	Initial	91.481	97.932		
847	C	-58.799	-49.259	1.574	2.107
1424	A	41.947	65.604	0.000	0.837
8751	B	137.116	107.987	0.232	1.264

The dihedral angles (RC1 and RC2), potential of mean force (PMF), and root mean square displacement (RMSD) of the local minimum geometries obtained during the AMD simulation

From the dihedral angles it is evident that no parts of the molecule are orthogonal to each other, hence the delocalization of electron density over the dimethoxy acetophenon moiety stabilized towards the mechanism of formation of pyrimidines. Planarity of the methoxy groups is lost and the conformational orientation of methyl sulfanyl groups and the aldehydic moiety appears to be changed with respect to AMD based conformations and there are no intermolecular interactions associated with these conformations.

3.4 Natural Bond Orbital Analysis

The Natural Bond Orbital (NBO) calculations were performed using Gaussian09 software package with B3LYP/6-31G(d,p) method. It offers a valuable platform for exploring charge transfer or conjugative interaction in molecular systems and is an efficient method for studying molecular bonding characteristics and interaction among bonds. The larger the stabilization energy value, the more intensive is the interaction between electron donors and electron acceptors, i.e. the more donating tendency from electron donors to electron acceptors and the greater the extent of conjugation of the whole system. The NBO analysis is already proved to be an effective tool for chemical interpretation of hyperconjugative interaction and electron density transfer from the filled lone pair electron. The second order Fock matrix was carried out to evaluate donor (i)–acceptor (j) interaction in the NBO analysis [29]. For each donor (i) and acceptor (j) the stabilization energy E(2) associated with the delocalization i to j is as follows:

$$E(2) = \Delta E_{ij} = q_i \frac{(F_{ij})^2}{(E_j - E_i)}$$

Where q_i is the donor orbital occupancy, E_i and E_j are the diagonal elements and F_{ij} is the off diagonal NBO Fock matrix element. In NBO analysis large E(2) value shows the intensive interaction between electron-donors and electron-acceptors and if it is large, greater the

extent of conjugation of the whole system. The possible intensive interactions are given in **Table 5**.

Table 5

Second order perturbation theory analysis of Fock matrix in NBO basis for NDDP

	Donar (i)	Type	ED (i) e		Acceptor (j)	Type	ED (j) e	E(2)[a] (KJ mol^{-1})	E(j)-E(i)[b] (a.u.)	F(i,j)[c] (a.u.)
BD	C 1 - C 2	σ	1.97054	BD*	C 1 - C 3	σ*	0.02187	3.78	1.26	0.062
BD	C 1 - C 2	σ	1.97054	BD*	C 1 - C 8	σ*	0.06229	1.86	1.15	0.042
BD	C 1 - C 2	σ	1.97054	BD*	C 2 - C 4	σ*	0.02392	3	1.26	0.055
BD	C 1 - C 2	σ	1.97054	BD*	C 2 - H 22	σ*	0.01423	1.53	1.17	0.038
BD	C 1 - C 2	σ	1.97054	BD*	C 3 - H 23	σ*	0.01499	2.05	1.18	0.044
BD	C 1 - C 2	σ	1.97054	BD*	C 4 - O 20	σ*	0.02592	4.82	1.06	0.064
BD	C 1 - C 2	σ	1.97054	BD*	C 8 - O 9	σ*	0.01491	1.89	1.26	0.044
BD	C 1 - C 3	σ	1.64644	BD*	C 1 - C 2	σ*	0.0219	3.67	1.25	0.061
BD	C 1 - C 3	σ	1.64644	BD*	C 1 - C 8	σ*	0.06229	2.33	1.15	0.047
BD	C 1 - C 3	σ	1.64644	BD*	C 2 - H 22	σ*	0.01423	2.16	1.17	0.045
BD	C 1 - C 3	σ	1.64644	BD*	C 3 - C 5	σ*	0.01313	2.41	1.28	0.05
BD	C 1 - C 3	σ	1.64644	BD*	C 3 - H 23	σ*	0.01499	1.21	1.18	0.034
BD	C 1 - C 3	σ	1.64644	BD*	C 5 - H 24	σ*	0.01232	2.28	1.17	0.046
BD	C 1 - C 3	σ	1.64644	BD*	C 8 - C 10	σ*	0.07164	2.14	1.08	0.044
BD	C 1 - C 3	π	1.64644	BD*	C 1 - C 3	π*	0.39062	0.54	0.28	0.011
BD	C 1 - C 3	π	1.64644	BD*	C 2 - C 4	π*	0.3524	20.52	0.27	0.067
BD	C 1 - C 3	π	1.64644	BD*	C 5 - C 6	π*	0.38483	17.83	0.27	0.062
BD	C 1 - C 3	π	1.64644	BD*	C 8 - O 9	π*	0.16842	23.35	0.26	0.073
BD	C 1 - C 8	σ	1.9784	BD*	C 1 - C 2	σ*	0.0219	2.47	1.24	0.049
BD	C 1 - C 8	σ	1.9784	BD*	C 1 - C 3	σ*	0.02187	2.24	1.25	0.047
BD	C 1 - C 8	σ	1.9784	BD*	C 2 - C 4	σ*	0.02392	2	1.25	0.045
BD	C 1 - C 8	σ	1.9784	BD*	C 3 - C 5	σ*	0.01313	2.14	1.26	0.046
BD	C 1 - C 8	σ	1.9784	BD*	C 8 - O 9	σ*	0.01491	0.63	1.24	0.025
BD	C 1 - C 8	σ	1.9784	BD*	C 8 - C 10	σ*	0.07164	0.51	1.06	0.021
BD	C 1 - C 8	σ	1.9784	BD*	C 10 - C 11	σ*	0.03039	0.79	1.25	0.028
BD	C 1 - C 8	σ	1.9784	BD*	C 10 - C 11	π*	0.26554	0.79	0.67	0.022
BD	C 2 - C 4	σ	1.97893	BD*	C 1 - C 2	σ*	0.0219	3.27	1.28	0.058
BD	C 2 - C 4	σ	1.97893	BD*	C 1 - C 8	σ*	0.06229	2.96	1.18	0.053
BD	C 2 - C 4	σ	1.97893	BD*	C 2 - H 22	σ*	0.01423	1.45	1.2	0.037
BD	C 2 - C 4	σ	1.97893	BD*	C 4 - C 6	σ*	0.03362	3.5	1.24	0.059
BD	C 2 - C 4	σ	1.97893	BD*	C 6 - O 7	σ*	0.02503	2.64	1.1	0.048
BD	C 2 - C 4	π	1.70466	BD*	C 1 - C 3	π*	0.39062	16.76	0.3	0.065
BD	C 2 - C 4	π	1.70466	BD*	C 5 - C 6	π*	0.38483	18.55	0.29	0.067
BD	C 2 - H 22	σ	1.97441	BD*	C 1 - C 2	σ*	0.0219	1.17	1.09	0.032
BD	C 2 - H 22	σ	1.97441	BD*	C 1 - C 3	σ*	0.02187	3.93	1.11	0.059
BD	C 2 - H 22	σ	1.97441	BD*	C 2 - C 4	σ*	0.02392	1.18	1.11	0.032
BD	C 2 - H 22	σ	1.97441	BD*	C 4 - C 6	σ*	0.03362	4.4	1.05	0.061
BD	C 2 - H 22	σ	1.97441	BD*	C 4 - O 20	σ*	0.02592	0.54	0.9	0.02
BD	C 3 - C 5	σ	1.97552	BD*	C 1 - C 3	σ*	0.02187	2.91	1.27	0.054
BD	C 3 - C 5	σ	1.97552	BD*	C 1 - C 8	σ*	0.06229	3.15	1.16	0.054
BD	C 3 - C 5	σ	1.97552	BD*	C 3 - H 23	σ*	0.01499	1.24	1.19	0.034
BD	C 3 - C 5	σ	1.97552	BD*	C 5 - C 6	σ*	0.02569	2.82	1.25	0.053
BD	C 3 - C 5	σ	1.97552	BD*	C 5 - H 24	σ*	0.01232	1.51	1.18	0.038
BD	C 3 - C 5	σ	1.97552	BD*	C 6 - O 7	σ*	0.02503	4.65	1.08	0.063
BD	C 3 - H 23	σ	1.9798	BD*	C 1 - C 2	σ*	0.0219	4.45	1.08	0.062
BD	C 3 - H 23	σ	1.9798	BD*	C 1 - C 3	σ*	0.02187	1.14	1.09	0.031
BD	C 3 - H 23	σ	1.9798	BD*	C 3 - C 5	σ*	0.01313	0.97	1.11	0.029
BD	C 3 - H 23	σ	1.9798	BD*	C 5 - C 6	σ*	0.02569	3.92	1.07	0.058
BD	C 4 - C 6	σ	1.96977	BD*	C 2 - C 4	σ*	0.02392	3.07	1.28	0.056
BD	C 4 - C 6	σ	1.96977	BD*	C 2 - H 22	σ*	0.01423	2.24	1.18	0.046
BD	C 4 - C 6	σ	1.96977	BD*	C 5 - C 6	σ*	0.02569	2.8	1.26	0.053
BD	C 4 - C 6	σ	1.96977	BD*	C 5 - H 24	σ*	0.01232	2.07	1.18	0.044
BD	C 4 - C 6	σ	1.96977	BD*	O 7 - C 19	σ*	0.0084	2.99	0.98	0.049
BD	C 4 - C 6	σ	1.96977	BD*	O 20 - C 21	σ*	0.00791	2.81	0.99	0.047
BD	C 4 - O 20	σ	1.99122	BD*	C 1 - C 2	σ*	0.0219	1.2	1.46	0.038
BD	C 4 - O 20	σ	1.99122	BD*	C 2 - C 4	σ*	0.02392	1.1	1.48	0.036
BD	C 4 - O 20	σ	1.99122	BD*	C 5 - C 6	σ*	0.02569	1.6	1.46	0.043
BD	C 4 - O 20	σ	1.99122	BD*	C 21 - H 36	σ*	0.00706	0.61	1.37	0.026
BD	C 5 - C 6	σ	1.97999	BD*	C 3 - C 5	σ*	0.01313	2.73	1.3	0.053
BD	C 5 - C 6	σ	1.97999	BD*	C 3 - H 23	σ*	0.01499	2.06	1.2	0.045
BD	C 5 - C 6	σ	1.97999	BD*	C 4 - C 6	σ*	0.03362	3.25	1.23	0.057
BD	C 5 - C 6	σ	1.97999	BD*	C 4 - O 20	σ*	0.02592	2.74	1.09	0.049
BD	C 5 - C 6	σ	1.97999	BD*	C 5 - H 24	σ*	0.01232	1.16	1.2	0.033
BD	C 5 - C 6	π	1.65568	BD*	C 1 - C 3	π*	0.39062	22.33	0.3	0.074
BD	C 5 - C 6	π	1.65568	BD*	C 2 - C 4	π*	0.3524	16.67	0.29	0.062
BD	C 5 - C 6	π	1.65568	BD*	C 5 - C 6	π*	0.38483	0.87	0.28	0.014
BD	C 5 - H 24	σ	1.97694	BD*	C 1 - C 3	σ*	0.02187	3.69	1.1	0.057
BD	C 5 - H 24	σ	1.97694	BD*	C 3 - C 5	σ*	0.01313	1.13	1.11	0.032
BD	C 5 - H 24	σ	1.97694	BD*	C 4 - C 6	σ*	0.03362	4.3	1.04	0.06
BD	C 5 - H 24	σ	1.97694	BD*	C 5 - C 6	σ*	0.02569	0.95	1.08	0.029
BD	C 5 - H 24	σ	1.97694	BD*	C 6 - O 7	σ*	0.02503	0.52	0.91	0.019
BD	C 6 - O 7	σ	1.9918	BD*	C 2 - C 4	σ*	0.02392	1.59	1.49	0.044
BD	C 6 - O 7	σ	1.9918	BD*	C 3 - C 5	σ*	0.01313	1.04	1.5	0.035
BD	C 6 - O 7	σ	1.9918	BD*	C 5 - C 6	σ*	0.02569	0.97	1.47	0.034
BD	C 6 - O 7	σ	1.9918	BD*	C 19 - H 32	σ*	0.00684	0.54	1.38	0.024
BD	O 7 - C 19	σ	1.99201	BD*	C 4 - C 6	σ*	0.03362	3.06	1.33	0.057
BD	C 8 - O 9	σ	1.99437	BD*	C 1 - C 2	σ*	0.0219	1.29	1.63	0.041
BD	C 8 - O 9	σ	1.99437	BD*	C 1 - C 8	σ*	0.06229	1.17	1.53	0.038
BD	C 8 - O 9	σ	1.99437	BD*	C 8 - C 10	σ*	0.07164	0.73	1.46	0.03
BD	C 8 - O 9	σ	1.99437	BD*	C 10 - C 11	π*	0.26554	0.51	1.06	0.022
BD	C 8 - O 9	π	1.97319	BD*	C 1 - C 3	π*	0.39062	3.63	0.41	0.038

BD	C 8 - O 9	π	1.97319	BD*	C 10 - C 11	σ*	0.03039	1.54	0.96	0.034
BD	C 8 - O 9	π	1.97319	BD*	C 10 - C 16	σ*	0.0605	1.49	0.83	0.032
BD	C 8 - O 9	π	1.97319	BD*	S 12 - C 14	σ*	0.01247	0.59	0.53	0.016
BD	C 8 - C 10	σ	1.96748	BD*	C 1 - C 3	σ*	0.02187	2.37	1.22	0.048
BD	C 8 - C 10	σ	1.96748	BD*	C 1 - C 8	σ*	0.06229	0.56	1.11	0.022
BD	C 8 - C 10	σ	1.96748	BD*	C 10 - C 11	σ*	0.03039	3.21	1.23	0.056
BD	C 8 - C 10	σ	1.96748	BD*	C 10 - C 16	σ*	0.0605	0.77	1.1	0.026
BD	C 8 - C 10	σ	1.96748	BD*	C 11 - S 13	σ*	0.04841	4.84	0.81	0.056
BD	C 8 - C 10	σ	1.96748	BD*	C 16 - H 18	σ*	0.05791	1.67	1.07	0.038
BD	C 10 - C 11	σ	1.98187	BD*	C 1 - C 8	σ*	0.06229	0.61	1.24	0.025
BD	C 10 - C 11	σ	1.98187	BD*	C 8 - O 9	π*	0.16842	0.66	0.79	0.021
BD	C 10 - C 11	σ	1.98187	BD*	C 8 - C 10	σ*	0.07164	2.71	1.17	0.051
BD	C 10 - C 11	σ	1.98187	BD*	C 10 - C 16	σ*	0.0605	2.69	1.24	0.052
BD	C 10 - C 11	σ	1.98187	BD*	C 11 - S 12	σ*	0.056	0.56	0.95	0.021
BD	C 10 - C 11	σ	1.98187	BD*	C 11 - S 13	σ*	0.04841	0.58	0.94	0.021
BD	C 10 - C 11	σ	1.98187	BD*	C 16 - O 17	σ*	0.00462	1.02	1.36	0.033
BD	C 10 - C 11	π	1.8445	BD*	C 1 - C 8	σ*	0.06229	2.44	0.76	0.039
BD	C 10 - C 11	π	1.8445	BD*	C 8 - O 9	σ*	0.01491	3.7	0.87	0.052
BD	C 10 - C 11	π	1.8445	BD*	C 8 - O 9	π*	0.16842	0.99	0.31	0.016
BD	C 10 - C 11	π	1.8445	BD*	C 10 - C 11	π*	0.26554	3.49	0.3	0.03
BD	C 10 - C 11	π	1.8445	BD*	S 12 - C 14	σ*	0.01247	0.73	0.45	0.017
BD	C 10 - C 11	π	1.8445	BD*	S 13 - C 15	σ*	0.01233	1.47	0.44	0.024
BD	C 10 - C 11	π	1.8445	BD*	C 16 - O 17	π*	0.16429	21.37	0.3	0.072
BD	C 10 - C 16	σ	1.9734	BD*	C 8 - O 9	σ*	0.01491	0.57	1.25	0.024
BD	C 10 - C 16	σ	1.9734	BD*	C 8 - O 9	π*	0.16842	1.79	0.7	0.033
BD	C 10 - C 16	σ	1.9734	BD*	C 8 - C 10	σ*	0.07164	0.73	1.08	0.025
BD	C 10 - C 16	σ	1.9734	BD*	C 10 - C 11	σ*	0.03039	3.91	1.27	0.063
BD	C 10 - C 16	σ	1.9734	BD*	C 11 - S 12	σ*	0.056	3.81	0.86	0.051
BD	C 11 - S 12	σ	1.98053	BD*	C 10 - C 11	σ*	0.03039	1.26	1.25	0.036
BD	C 11 - S 12	σ	1.98053	BD*	C 10 - C 16	σ*	0.0605	4.46	1.12	0.064
BD	C 11 - S 12	σ	1.98053	BD*	S 12 - C 14	σ*	0.01247	0.59	0.82	0.02
BD	C 11 - S 12	σ	1.98053	BD*	C 14 - H 26	σ*	0.00592	0.68	1.12	0.025
BD	C 11 - S 13	σ	1.97876	BD*	C 8 - C 10	σ*	0.07164	4.18	1.05	0.06
BD	C 11 - S 13	σ	1.97876	BD*	C 10 - C 11	σ*	0.03039	1.83	1.24	0.043
BD	C 11 - S 13	σ	1.97876	BD*	S 13 - C 15	σ*	0.01233	0.54	0.8	0.019
BD	C 11 - S 13	σ	1.97876	BD*	C 15 - H 30	σ*	0.00486	0.8	1.11	0.027
BD	S 12 - C 14	σ	1.98765	BD*	C 10 - C 11	σ*	0.03039	1.97	1.19	0.043
BD	S 12 - C 14	σ	1.98765	BD*	C 11 - S 12	σ*	0.056	0.63	0.78	0.02
BD	S 13 - C 15	σ	1.97881	BD*	C 10 - C 11	π*	0.26554	2.01	0.6	0.033
BD	S 13 - C 15	σ	1.97881	BD*	C 11 - S 12	σ*	0.056	1.44	0.77	0.03
BD	S 13 - C 15	σ	1.97881	BD*	C 11 - S 13	σ*	0.04841	0.56	0.76	0.019
BD	C 14 - H 26	σ	1.98634	BD*	C 11 - S 12	σ*	0.056	2.16	0.7	0.035
BD	C 15 - H 30	σ	1.98666	BD*	C 11 - S 13	σ*	0.04841	1.96	0.69	0.033
BD	C 16 - O 17	σ	1.99645	BD*	C 10 - C 11	σ*	0.03039	1.48	1.64	0.044
BD	C 16 - O 17	σ	1.99645	BD*	C 10 - C 16	σ*	0.0605	0.79	1.51	0.031
BD	C 16 - O 17	π	1.97373	BD*	C 10 - C 11	π*	0.26554	6.34	0.38	0.046
BD	C 16 - H 18	σ	1.98603	BD*	C 8 - C 10	σ*	0.07164	3.55	0.94	0.052
BD	C 19 - H 32	σ	1.99074	BD*	C 6 - O 7	σ*	0.02503	3.38	0.9	0.05
BD	O 20 - C 21	σ	1.99211	BD*	C 4 - C 6	σ*	0.03362	3.06	1.33	0.057
BD	C 21 - H 36	σ	1.99047	BD*	C 4 - O 20	σ*	0.02592	3.42	0.89	0.05
LP	O 7	σ	1.96479	BD*	C 4 - C 6	σ*	0.03362	0.91	1.07	0.028
LP	O 7	σ	1.96479	BD*	C 5 - C 6	σ*	0.02569	7.47	1.11	0.081
LP	O 7	σ	1.96479	BD*	C 19 - H 31	σ*	0.0168	1.13	0.99	0.03
LP	O 7	σ	1.96479	BD*	C 19 - H 32	σ*	0.00684	1.74	1.02	0.038
LP	O 7	σ	1.96479	BD*	C 19 - H 33	σ*	0.01678	1.13	0.99	0.03
LP	O 7	π	1.81946	BD*	C 5 - C 6	π*	0.38483	33.28	0.34	0.1
LP	O 7	π	1.81946	BD*	C 19 - H 31	σ*	0.0168	4.87	0.76	0.057
LP	O 7	π	1.81946	BD*	C 19 - H 33	σ*	0.01678	4.87	0.76	0.057
LP	O 9	σ	1.97765	BD*	C 1 - C 8	σ*	0.06229	2.48	1.15	0.048
LP	O 9	σ	1.97765	BD*	C 8 - C 10	σ*	0.07164	1.26	1.09	0.033
LP	O 9	π	1.88563	BD*	C 1 - C 8	σ*	0.06229	17.21	0.73	0.101
LP	O 9	π	1.88563	BD*	C 8 - C 10	σ*	0.07164	20.51	0.66	0.105
LP	O 9	π	1.88563	BD*	C 10 - C 11	π*	0.26554	1.03	0.26	0.015
LP	S 12	σ	1.9763	BD*	C 10 - C 11	π*	0.26554	0.54	0.63	0.018
LP	S 12	σ	1.9763	BD*	C 11 - S 13	σ*	0.04841	4.67	0.79	0.055
LP	S 12	σ	1.9763	BD*	C 14 - H 25	σ*	0.0111	0.77	1.09	0.026
LP	S 12	σ	1.9763	BD*	C 14 - H 27	σ*	0.01285	0.83	1.09	0.027
LP	S 12	π	1.78576	BD*	C 8 - O 9	π*	0.16842	0.71	0.26	0.012
LP	S 12	π	1.78576	BD*	C 10 - C 11	σ*	0.03039	0.84	0.84	0.025
LP	S 12	π	1.78576	BD*	C 10 - C 11	π*	0.26554	20.39	0.25	0.065
LP	S 12	π	1.78576	BD*	C 11 - S 13	σ*	0.04841	1.12	0.42	0.02
LP	S 12	π	1.78576	BD*	C 14 - H 25	σ*	0.0111	2.89	0.71	0.043
LP	S 12	π	1.78576	BD*	C 14 - H 27	σ*	0.01285	3.35	0.72	0.046
LP	S 13	σ	1.9793	BD*	C 10 - C 11	σ*	0.03039	3.43	1.21	0.058
LP	S 13	σ	1.9793	BD*	C 15 - H 28	σ*	0.01513	1.24	1.08	0.033
LP	S 13	π	1.86534	BD*	C 10 - C 11	σ*	0.03039	2.03	0.85	0.038
LP	S 13	π	1.86534	BD*	C 10 - C 11	π*	0.26554	7.18	0.26	0.04
LP	S 13	π	1.86534	BD*	C 11 - S 12	σ*	0.056	5.68	0.44	0.046
LP	S 13	π	1.86534	BD*	C 14 - H 26	σ*	0.00592	0.6	0.72	0.019
LP	S 13	π	1.86534	BD*	C 15 - H 28	σ*	0.01513	3.28	0.72	0.045
LP	S 13	π	1.86534	BD*	C 15 - H 29	σ*	0.01123	3.17	0.72	0.044
LP	S 13	π	1.86534	BD*	C 16 - H 18	σ*	0.05791	1.29	0.69	0.027
LP	O 17	σ	1.98322	BD*	C 10 - C 16	σ*	0.0605	1.5	1.16	0.038
LP	O 17	σ	1.98322	BD*	C 16 - H 18	σ*	0.05791	1.2	1.12	0.033
LP	O 17	π	1.89528	BD*	C 8 - O 9	π*	0.16842	1.21	0.28	0.017
LP	O 17	π	1.89528	BD*	C 10 - C 16	σ*	0.0605	19.21	0.72	0.106
LP	O 17	π	1.89528	BD*	C 16 - H 18	σ*	0.05791	19.36	0.69	0.104
LP	O 20	σ	1.96457	BD*	C 2 - C 4	σ*	0.02392	7.44	1.12	0.082
LP	O 20	σ	1.96457	BD*	C 4 - C 6	σ*	0.03362	0.87	1.07	0.027
LP	O 20	σ	1.96457	BD*	C 21 - H 34	σ*	0.01833	1.15	0.99	0.03
LP	O 20	σ	1.96457	BD*	C 21 - H 35	σ*	0.01808	1.17	0.99	0.031
LP	O 20	σ	1.96457	BD*	C 21 - H 36	σ*	0.00706	1.74	1.02	0.038
LP	O 20	π	1.8409	BD*	C 2 - C 4	π*	0.3524	30.91	0.34	0.096
LP	O 20	π	1.8409	BD*	C 21 - H 34	σ*	0.01833	5.16	0.75	0.058
LP	O 20	π	1.8409	BD*	C 21 - H 35	σ*	0.01808	5.09	0.75	0.057

BD*	C 5 - C 6	π*	0.38483	BD*	C 1 - C 3	π*	0.39062	260.5	0.01	0.082
BD*	C 8 - O 9	π*	0.16842	BD*	C 1 - C 3	π*	0.39062	81.62	0.02	0.075
BD*	C 8 - O 9	π*	0.16842	BD*	C 10 - C 11	σ*	0.03039	0.72	0.57	0.058
BD*	C 8 - O 9	π*	0.16842	BD*	C 10 - C 16	σ*	0.0605	0.98	0.45	0.055
BD*	C 10 - C 11	π*	0.26554	BD*	C 1 - C 8	σ*	0.06229	0.96	0.46	0.047
BD*	C 10 - C 11	π*	0.26554	BD*	C 8 - O 9	σ*	0.01491	1.16	0.57	0.061
BD*	C 10 - C 11	π*	0.26554	BD*	C 8 - O 9	π*	0.16842	4.91	0.01	0.015
BD*	C 10 - C 11	π*	0.26554	BD*	S 13 - C 15	σ*	0.01233	1.5	0.14	0.035

[a]E(2) means energy of hyperconjugative interactions (stabilization energy in kcal/mol).
[b]Energy difference between donor and acceptor I and j NBO orbitals in a.u.
[c]F(ij) is the Fock matrix elements between I and j NBO orbitals in a.u

The resonance stabilization of molecule can be rationalised through the interaction of various orbitals. The aromatic system having extensive conjugation over π systems as evident with the interaction of π^*(C5-C6) to π^*(C1-C3), having a strong stabilization energy of 260.5 kcal mol^{-1}. Conjugative interaction of π(C5-C6) to π^*(C1-C3) and π^*(C2-C4) leads to a stabilization energies of 22.33 and 16.67 kcal mol^{-1} respectively. The interaction of π(C2-C4) to π^*(C1-C3) and π^*(C5-C6) along with π(C1-C3) to π^*(C2-C4), π^*(C5-C6) also favours the aromatic delocalization of electron density with stabilization energies 16.76, 18.55, 20.52 and 17.83 kcal mol^{-1} respectively. The electron releasing effect of methoxy group and its contribution to the aromatic system can be rationalized through the interaction of π(O20) and π^*(C2-C4) along with π(O7) and π^*(C5-C6) with a stabilization of 30.91 and 33.28 kcal mol^{-1}. Among the two sulphur atoms, S12 is more stable because of the delocalization with π^*(C10-O11) having stabilization energy of 20.39 kcal mol^{-1} where as S13 interact with the same orbital with an energy of 7.18 kcal mol^{-1}, therefore the leaving methyl thiol could be contain S13 on reacting with amidines. This interaction is also favours by contribution from π(O17) to σ^*(C10-C16) lead to conjugation. π(C1-C3) to π^*(C8-O9) reveals the extension of conjugation over the ketonic carbonyl group leading to the formation of cyclic intermediate through 1,2-nucleophilic addition leads to the formation of pyrimidine with a stabilization energy of 23.35 kcal mol^{-1}, this interaction favours the back donation of π^*(C8-O9) to π^*(C1-C3) with strong stabilization of 81.62 kcal mol^{-1}. And the ketonic carbonyl acts as a electron delocalization bridge as evident by the interaction of π(O9) with σ^*(C8-C10) and σ^*(C1-C8) along with a stabilization energy 20.51 and 17.21 kcal mol^{-1}.

3.5 Mulliken Population Analyses

The calculation of atomic charges plays an important role in the application of quantum mechanical calculations to molecular systems [30]. Our interest here is to describe the electron distribution in Mol1 as broadly as possible. Mulliken charges were calculated by determining the electron population of each atom for its activity assessment towards the formation of pyrimidines derivatives. The Mulliken plot corresponding with B3LYP with 6-311++G(d,p) method is shown in **Fig. 8**

Figure 8

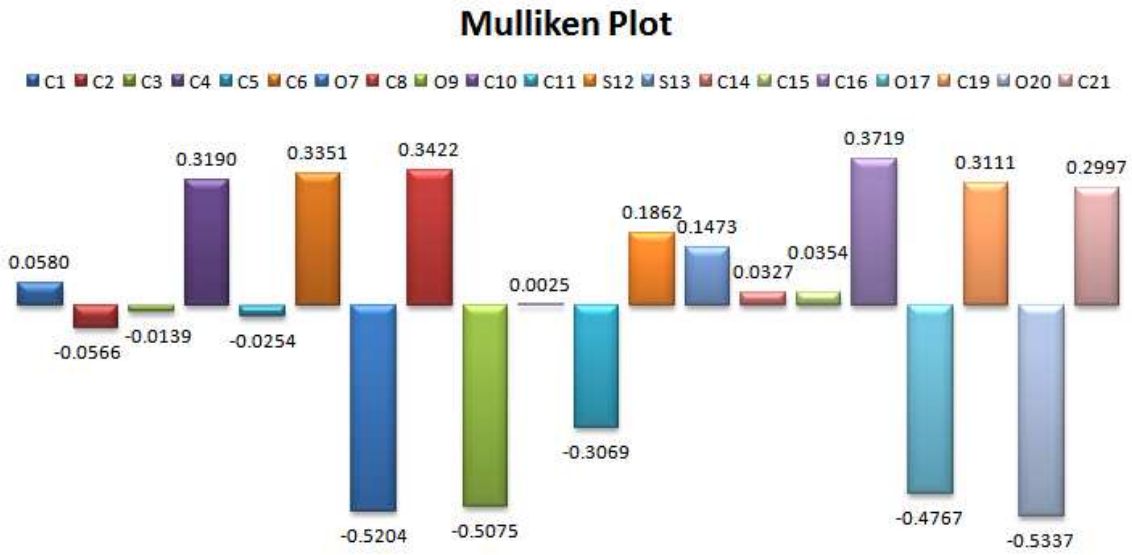

Mullikan population analysis based on the optimized structure reveals the partial charge density of formyl ketenedithioacetal represented in Table IV. The atom C11 is highly electronegative whereas C10 is electropositive reveals the extensive charge delocalization, the decrease in bond length also support this. Substituted aromatic carbon atoms are positively charged, where C1 shows less positive as 0.0579e due to the presence of electron withdrawing effect of ketonic carbonyl moiety, as compared to C4 and C6 with 0.319e and 0.335e respectively, due to the attachment of electron releasing methoxy groups. C2, C3 and C5 are the unsubtituted aromatic carbon atoms with negative population as -0.0565e, -0.0139e and -0.0254e respectively shows the electronic delocalization within the ring and extended to the whole molecule through conjugation. Both ketonic and aldehydic oxygen atoms are highly electronegative as -0.5075 and -0.4766e respectively and the corresponding bonded carbon atoms are positively populated, viz. C8 (0.3422e) and C16 (0.3719e) is also an evidence for electronic delocalization leading to charge transfer between the aromatic system and rest of the fractions through ketonic carbonyl group

The trigonal planar carbon (C11 -0.3068) with lack of non-bonded interaction supports the mechanism by releasing methyl thiol leading to the formation of pyrimidines where C14 and C15 are being in non-bonded interactions (from crystallographic data). Ketonic carbonyl oxygen is highly polarized with a density of -0.5075e leads to make the hydroxyl moiety in the intermediate structure followed by the removal of the same as water. The aldehydic oxygen is also highly populated but this is unreacted over the reaction is due to the extensive non-covalent interactions with various less populated atoms (Fig. 4). This

interaction may brakes once pyrimidine is formed and the aldehyde facile to Konevenangel condensation yielding functionalized pyridines.

3.6 Fukui function analysis

The Fukui function is among the most basic and commonly used reactivity descriptors. The Fukui function is given as the change in the density function *ρ(r)* for the molecule as a consequence of changing the number of electrons N in the molecule, under the constraint of a constant external potential. The Fukui function is defined as:

$$F(r) = \left(\frac{\partial \rho(\mathrm{r})}{\partial \mathrm{N}}\right)\mathrm{r}$$

Where *ρ(r)* is the electronic density, N is the number of electrons and r is the external potential exerted by the nuclease. Fukui functions are introduced, which are prescribed as reactivity descriptors in order to identify the most reactive sites for electrophilic or nucleophilic reactions within the molecule. The Fukui function indicates the susceptibility of electronic density to deform at a given position upon accepting or donating electrons [31, 32]. Also, it is possible to define the corresponding condensed or atomic Fukui functions [33] on the j^{th} atom site as,

$$f_j^- = q_j(N) - q_j(N-1)$$

$$f_j^+ = q_j(N+1) - q_j(N)$$

$$f_j^0 = \frac{1}{2}\left[q_j(N+1) - q_j(N-1)\right]$$

For an electrophilic $f_j^-(r)$, nucleophilic $f_j^+(r)$ and free radical attack $f_j^0(r)$ on the reference molecule, respectively. In these equations, q_j is the atomic charge (electrostatic derived charge) at the j^{th} atomic site in the neutral (N), anionic (N + 1) or cationic (N - 1) chemical species.

The electrophilicity of the atoms is in the order of C8 > C15 > C14 > C1 > C11 > C21> C19 > C5 > H22, whereas nucleophilic character is C3 > C4 > C1 > C6 > O20 > O7 > O9 > H34 > H35 > H33 > H31 > S12 > S13 > H32 > H36 > H22 > O17 > C2 > H23 > H18 = H30 > H25 > H26 > H27 > H28 > H29 > C8. Radical nature could be S12 > S13 > C3 > C10 > C16 > O17 > C4 > O9 > C6 > O20 > O7 > C1 > H30 > H34 > H26 > H31 > H29 > H35 > H33 > H31 > H32 > H36 > H24 > H18 > H25 > H28 > H27 > H23 > C2 > H22. The formation of pyrimidine can be explained on the basis of Fukui parameters (**Table 6**). The initial amidine nucleophile can simply attack on C14 since it is a good electrophilic centre (-0.0278) whereas the two sulphur atoms are merely nucleophilic in nature as evidenced with Table 1, followed by 1,2 cycloaddition also favours the electrophilic character of C11(-

0.1332) and it is due to the delocalization of electron density over acetophenon moiety. The aldehydic carbon (C25) exist as nucleophilic centre hence it is unreactive over the formation of pyrimidine and susceptible for yielding highly functionalised pyrimidine derivatives through Konevenangel condensation [28]. Mulliken population and Natural Bond Orbial analysis support these phenomena. Both methoxy oxygen atoms are less nucleophilic in nature as O10 is 0.0825 and O32 is 0.0911 because of the contribution of electron density towards aromatic ring.

Table 6

Atoms	f-	f+	f0
C1	-0.0234	0.1010	0.0776
C2	0.0008	0.0116	0.0123
H22	-0.0144	0.0157	0.0014
C3	0.0529	0.1480	0.2009
H23	0.0007	0.0128	0.0136
C4	0.0129	0.1317	0.1446
C5	-0.0160	-0.0058	-0.0218
H24	0.0067	0.0279	0.0346
C6	0.0195	0.0966	0.1161
O7	0.0057	0.0825	0.0882
C8	-0.1332	0.0015	-0.1317
O9	0.0721	0.0611	0.1332
C10	0.2126	-0.0191	0.1936
C11	-0.0278	-0.0040	-0.0318
S12	0.1945	0.0345	0.2291
S13	0.1878	0.0299	0.2177
C14	-0.0368	-0.0147	-0.0514
H25	0.0236	0.0086	0.0322
H26	0.0428	0.0083	0.0511
H27	0.0126	0.0064	0.0189
C15	-0.0863	-0.0222	-0.1085
H28	0.0229	0.0062	0.0292
H29	0.0445	0.0060	0.0505
H30	0.0500	0.0099	0.0599
C16	0.1807	-0.0052	0.1755
H18	0.0246	0.0099	0.0345
O17	0.1482	0.0117	0.1599
C19	-0.0181	-0.0258	-0.0439
H31	0.0075	0.0357	0.0432
H32	0.0081	0.0281	0.0362
H33	0.0091	0.0358	0.0449
O20	0.0043	0.0911	0.0954
C21	-0.0230	-0.0184	-0.0414
34H	0.0148	0.0385	0.0534

35H	0.0109	0.0362	0.0471
36H	0.0081	0.0280	0.0361

Fukui parameters

3.7 Molecular Electrostatic Potential

MEP provides a visual medium to understand the relative reactivity of the molecule through its polarity, as shown in **Fig: 9**. MEP surface plot is a useful descriptive for the qualitative interpretation of the sites for electrophilic and nucleophilic attacks as well as hydrogen bonding interactions [34, 35]. The equation used to find the electrostatic potential is [36],

Total electrostatic potential energy = Σ Electrostatic Potential energy

Potential Energy = $k\frac{q1q2}{r}$ (k is the coulomb's constant)

The colours in the map correspond to the different potential values. Potential increases in the order of red < orange < yellow < green < blue, where blue indicates the strongest attraction; red indicates strongest repulsion; and green indicates neutral electrostatic potential region [37, 38]. From the figure it is evident that, the regions exhibiting the negative electrostatic potential are localized near the electronegative oxygen atoms while the regions presenting the positive potential are localized in the vicinity of the hydrogen atoms.

Aromatic pi electron density and its extension to ketonic carbonyl group can be seen from the figure where more negative potential is combines with ketonic carbonyl oxygen, so that corresponding carbon atom is more susceptible for nucleophilic attack reveals the formation of acyclic N,S-acetal. Aldehydic oxygen is also electron rich but it is inactive towards the formation of pyrimidine due to intermolecular interactions already explained in crystallographic part. Methoxy groups are electron releasing towards aromatic ring and hence it is less populated supports the mechanism of formation pyrimidines.

Figure 9

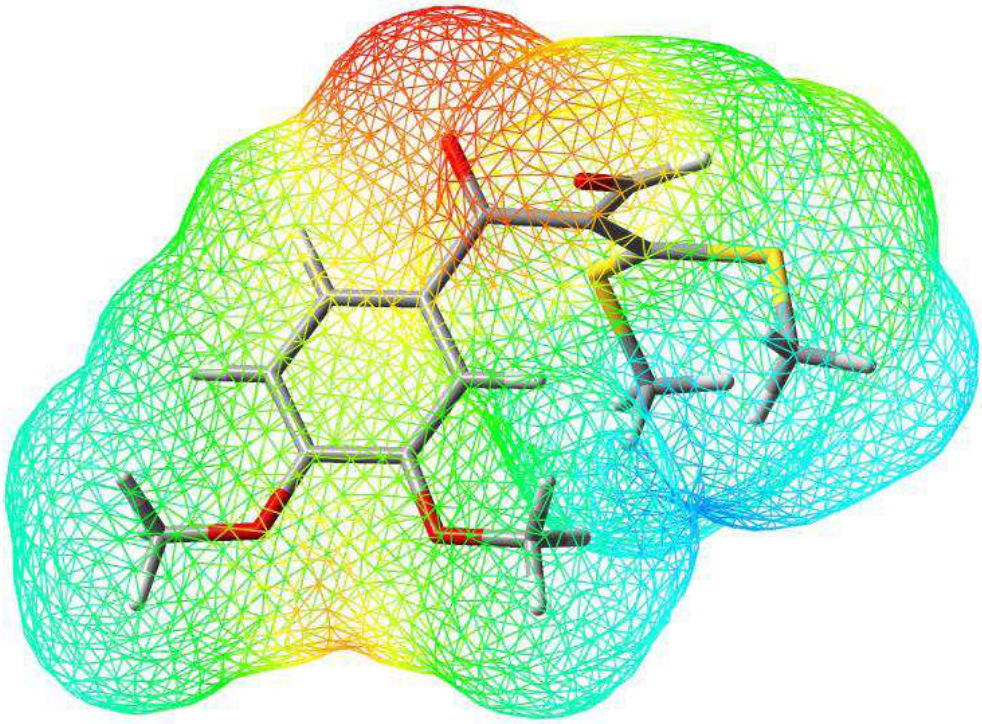

Electrostatic potential of the Mol1

3.8 Frontier Orbital Analysis

Highest occupied molecular orbital (HOMO) and lowest unoccupied molecular orbital (LUMO) are very important parameters for quantum chemistry. We can determine the way the molecule interacts with other species; hence, they are called the frontier orbitals. HOMO, which can be thought the outermost orbital containing electrons, tends to act as electron donor. On the other hand, LUMO can be thought the innermost orbital containing free places to accept electrons [39]

The highest occupied molecular orbital (HOMO) energies and lowest unoccupied molecular orbital (LUMO) energies have been calculated along with various other quantum mechanical descriptors viz. ionization energy (IE), chemical hardness (η), electronegativity (χ), total energy and dipole moment (Table V). Based on DFT-B3LYP model the total energy of the molecule calculated is -1640.333 a.u. IE can be expressed as the negative of HOMO orbital energy where as the negative of LUMO orbital energy corresponds to EA [33]. The chemical hardness (η) corresponds to the gap between HOMO-LUMO orbital energy. The larger the gap, harder is the molecule. HOMO-LUMO orbital energy gap (3.727eV) of the molecule reveals the thermodynamic stability of the system. The ionization potential obtained from theoretical calculation is also favours the stability of the molecule. The HOMO- LUMO

energy gap explicates the charge transfer interaction is taking place within the molecule. The calculated dipole moment value shows that the molecule is highly polar in nature. These calculated parameters are suitable for future applications of the Mol1.

Table 7

Quantum chemical reactivity descriptors

E_{HOMO} (eV) = -5.659
E_{LUMO} (eV) = -1.932
$E_{HOMO-LUMO}$ (eV) = 3.727
Total Energy (a.u.) = -1640.333
Ionization Potential (IE) = 5.659 eV
Electron Affinity (EA) = 1.932 eV
Global Electronegativity (χ) = 3.795 eV
Chemical Hardness (η) = 1.863 eV
Chemical Softness (S) = 0.536
Chemical Potential (μ) eV = -3.795
Global electrophilicity index (ω) = 3.865
Dipole Moment (Debye) = 4.955

3.9 Transition State (TS) Analysis

The Synchronous Transit-Guided Quasi-Newton (STQN) Method, developed by H. B. Schlegel *et al* [40], utilizes a linear synchronous transit or quadratic synchronous transit path way to get more proximate to the quadratic region around the transition state and then utilizes a quasi-Newton or eigenvector-following algorithm to consummate the optimization. As for minimizations, it performs optimizations by default utilizing redundant internal coordinates. This method will converge efficiently to the authentic transition structure utilizing an empirical estimate of the hessian and congruous starting structures.

Scheme 2

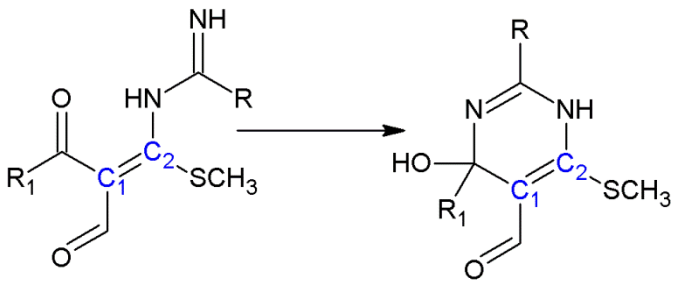

TS analysis performed between these two intermediates (from Figure 1)

Herein we performed QST3 [41] approach to simulate the transition state geometry between Scheme 2 with DFT-B3LYP/6-31+G(d,p) method. The imaginary frequency observed at -940.72 cm^{-1} show better correlation with the saddle point obtained with total energy of -1407.076 Hartree. HOMO-LUMO gap corresponding to the TS is 0.13517 Hartree reveal the easiness of internal rearrangement towards the formation of pyrimidines through this mechanism. The double bond between C_1 and C_2 (Scheme 2) is also support this mechanism via its rigidity toward rotation, hence the number of accessible geometry is limited for the acyclic N,S-acetal.

Figure 10

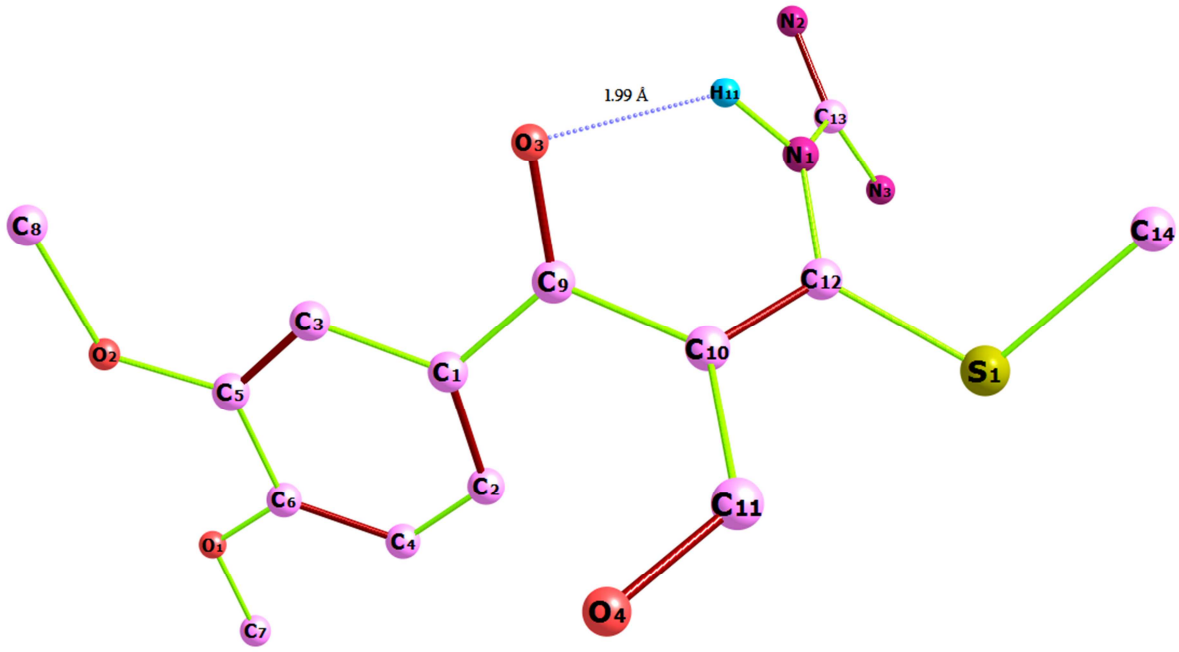

TS geometry of acyclic N,S-acetal with a hydrogen bonding interaction between O3 and H11, all other hydrogen atoms are omitted for clarity.

A strong hydrogen bonding interaction is observed between O3 and H11 (Figure 10) which is a characteristic feature of this TS towards its stability; and the over clouding electron density on ketonic carbonyl, inferred with MEP analysis of Mol1 is also supports this interaction. The aldehydic carbonyl moiety and the amidine groups make a torsion angle of -167.06° (C11-C10-C12-N2), hence it is confirmed as those groups are lying opposite to each other reveals the difficulties upon reacting towards the formation of cyclic intermediate via intramolecular 1,2-nucleophilic amination as described in the crystallographic part.

4. Conclusion

The present study dealt with ease of formation of pyrimidine derivatives from α-formylketene dithioacetal through electronic structure methods. Purposefully we synthesized the designated compound (Mol1) by a traditional method of synthesis from Asokan *et al* and characterized through spectral methods. Single crystal x-ray crystallographic study reveals the complete experimental structure as well as its intermolecular interactions; and show how it helps towards the formation functionalized pyrimidines. Classical and accelerated molecular dynamics simulation gave an insight into the possible conformational changes of the structure in acetonitrile environment and it discloses the various geometrical possibilities and interactions with the designated solvent system. Various quantum chemical reactivity parameters viz. NBO, Mulliken population, Fukui parameters, MEP, Frontier orbital analysis and TS analysis were carried out and it support the feasibility of formation of pyrimidines via ketonic carbonyl group rather than aldehydic carbonyl moiety.

Acknowledgements

Authors are thankful to SAIF CUSAT for data collection and IIRBS for NMR facilities. One of the authors Monu Joy gratefully acknowledged Kerala State Council for Science Technology and Environment (KSCSTE) for the financial support (No. 157/SPS/2013/CSTE).

References

[1] Anabha, E. R.; Nirmala, K. N.; Abraham, T.; Asokan, C. V., *Synthesis*, **2007**, 428.

[2] Anabha, E. R.; Asokan, C. V., *Synthesis*, **2006**, 151.

[3] Jutz, C. in *Advances in Organic Chemistry, Vol 9, Iminium Salts in Clrgunic Chemistry, Pnrr* Z Taylor, E. C. {ed) John Wiley, New York, 1 *976,* pp 225-342

[4] Koditz, J.; Rudorf, W. D.; Hartung, H.; Heinemann, F., *Liebigs. Ann. Chem.*, **1993**, 1003.

[5] Vinita Sharma, Nitin Chitranshi, and Ajay Kumar Agarwal, International Journal of Medicinal Chemistry, vol. 2014, Article ID 202784, 31 pages, 2014. doi:10.1155/2014/202784

[6] Mathew B*, Suresh J, Vinod D. Med Chem Res 2013; 22:3911–3917.

[7] Jung, M. H.; Park, J. G.; Yang, K. J.; Lee, M. J., Arch Pharm., 2001, 334, 79

[8] George, R. B.; David, M. H.; Elaine, S. E. S.; David, W.; David, S. C.; Allan, J. F.; Steven, C. G.; McTaggart, F.; Donald, J. M.; Graham, J. S.; Robin, W., J. Med. Chem., 2000, 43 ,4964.

[9] George, C. F., *Lancet.*, **2001**, *358*, 1623

[10] B. Mathew, A. Haridas, G. Uçar, I. Baysal, M. Joy, G. E. Mathew, B. Lakshmanan, V. Jayaprakash, *ChemMedChem* **2016**, 11, 1161

[11] Bruker (2012). SAINT. Bruker AXS Inc., Madison, Wisconsin, USA.

[12] Sheldrick, G. M. (1996). SADABS. University of Göttingen, Germany

[13] Sheldrick, G. M. (2015). *Acta Cryst.* A**71**, 3-8.

[14] Sheldrick, G. M. (2015). *Acta Cryst.* C**71**, 3-8

[15] Farrugia, L. J. (2012). *J. Appl. Cryst.* **45**, 849-854.

[16] Macrae, C. F., Edgington, P. R., McCabe, P., Pidcock, E., Shields, G. P., Taylor, R., Towler, M. & van de Streek, J. (2006). *J. Appl. Cryst.* **39**, 453-457.

[17] M. J. Frisch, G. W. Trucks, H. B. Schlegel, G. E. Scuseria, M. A. Robb, J. R. Cheeseman, G. Scalmani, V. Barone, B. Mennucci, G. A. Petersson, H. Nakatsuji, M. Caricato, X. Li, H. P. Hratchian, A. F. Izmaylov, J. Bloino, G. Zheng, J. L. Sonnenberg, M. Hada, M. Ehara, K. Toyota, R. Fukuda, J. Hasegawa, M. Ishida, T. Nakajima, Y. Honda, O. Kitao, H. Nakai, T. Vreven, J. A. Montgomery, Jr., J. E. Peralta, F. Ogliaro, M. Bearpark, J. J. Heyd, E. Brothers, K. N. Kudin, V. N. Staroverov, R. Kobayashi, J. Normand, K. Raghavachari, A. Rendell, J. C. Burant, S. S. Iyengar, J. Tomasi, M. Cossi, N. Rega, J. M. Millam, M. Klene, J. E. Knox, J. B. Cross, V. Bakken, C. Adamo, J. Jaramillo, R. Gomperts, R. E. Stratmann, O. Yazyev, A. J. Austin, R. Cammi, C. Pomelli, J. W. Ochterski, R. L. Martin, K. Morokuma, V. G. Zakrzewski, G. A. Voth, P. Salvador, J. J. Dannenberg, S. Dapprich, A. D. Daniels, Ö. Farkas, J. B. Foresman, J. V. Ortiz, J. Cioslowski, and D. J. Fox, Gaussian, Inc., Wallingford CT, 2009

[18] Dupradeau F-Y, Pigache A, Zaffran T, et al. The R.E.D. tools: advances in RESP and ESP charge derivation and force field library building. Phys Chem Chem Phys. 2010;12(28):7821-7839. doi:10.1039/c0cp00111b.

[19] Bijo Mathew, Abitha Haridas, Gülberk Uçar, Ipek Baysal, Adebayo A. Adeniyi, Mahmoud E.S. Soliman, Monu Joy, Githa Elizabeth Mathew, Baskar Lakshmanan, Venkatesan Jayaprakash. 91, (2016), 680-695. dx.doi.org/10.1016/j.ijbiomac.2016.05.110

[20] Case DA, Berryman JT, Betz RM, et al. AMBER 2015, University of California, San Francisco. 2015. citeulike-article-id:10779586.

[21] Götz AW, Williamson MJ, Xu D, Poole D, Le Grand S, Walker RC. Routine Microsecond Molecular Dynamics Simulations with AMBER on GPUs. 1. Generalized Born. J Chem Theory Comput. 2012;8(5):1542-1555. doi:10.1021/ct200909j.

[22] Ryckaert J-P, Ciccotti G, Berendsen HJC. Numerical integration of the cartesian equations of motion of a system with constraints: molecular dynamics of n-alkanes. J Comput Phys. 1977;23(3):327-341. doi:http://dx.doi.org/10.1016/0021-9991(77)90098-5.

[23] Miao Y, Sinko W, Pierce L, Bucher D, Walker RC, McCammon JA. Improved Reweighting of Accelerated Molecular Dynamics Simulations for Free Energy Calculation. J Chem Theory Comput. 2014;10(7):2677-2689. doi:10.1021/ct500090q.

[24] A.D. Becke, J.Chem.Phys. 98 (1993) 5648-5652

[25] C. Lee, W. Yang, R.G. Parr, Phys. Rev. B 37 (1988) 785-789

[26] NBO Version 3.1, E. D. Glendening, A. E. Reed, J. E. Carpenter, and F. Weinhold.

[27] Gompper, R.; Topfl, W., *Chem. Ber*.,**1962**, 95, 2871.

[28] Annie Mathews; Asokan C.V., *Tetrahedron*, 2007, 63, 33, 7845-7849.

[29] M. Szafran, A. Komasa, E.B. Adamska, J. Mol. Struct. (Theochem). 827 (2007) 101–107.

[30] R.S. Mulliken, J. Chem. Phys. 2 (1934) 782–793.

[31] R.G. Parr, W. Yang, Functional Theory of Atoms and Molecules, Oxford University Press, New York, 1989

[32] P.W. Ayers, R.G. Parr, J. Am. Chem. Soc. (2000) 2010–2018.

[33] C. Lee, W. Yang, R.G. Parr, J. Mol. Struct. THEOCHEM 163 (1988) 305e313.

[34] C. Parlak, M. Akdogan, G. Yildirim, N. Karagoz, E. Budak, C. Terzioglu, Spectrochim. Acta A Mol. Biomol. Spectrosc. 79 (2011) 263

[35] F.J. Luque, J.M. Lopez, M. Orozco, Theor. Chem. Acc. 103 (2000) 343.

[36] V. Arjunan, A. Jayaprakash, K. Carthigayan, S. Periandy, S. Mohan, Spectrochim. Acta A Mol. Biomol. Spectrosc. 108 (2013) 100.

[37] M. Kumru, V. Kucuk, M. Kocademir, H.M. Alfanda, A. Altun, L. Sari, Spectrochim. Acta A Mol. Biomol. Spectrosc. 134 (2015) 81.

[38] B.K. Paul, N. Guchhait, Comput. Theo. Chem. 1012 (2013) 20.

[39] G. Gece, Corros. Sci. 50 (2008) 2981

[40] C. Peng and H. B. Schlegel, "Combining Synchronous Transit and Quasi-Newton Methods to Find Transition States," *Israel J. of Chem.*, **33**, 449 (1993)

[41] A. Kanaani, D. Ajloo, H. Kiyani, M. Farahani. 1063, (2014), 30-44. dx.doi.org/10.1016/j.molstruc.2014.01.040

Highlights:

2-(3,4-dimethoxybenzoyl)-3,3-bis(methylsulfanyl)prop-2-enal is synthesised and characterized,

X-ray crystallography used to deduce experimental electronic structure and probable interactions

Classical and accelerated molecular dynamics simulation were carried out for conformational minima's

Various quantum chemical reactivity parameters were determined

Revealed the feasibility of one pot formation of pyrimidines through experimental and theoretical electronic structure